

Slurry-Phase Hydrogenation of Different Asphaltenes to Liquid Fuels on Dispersed MoS₂ Nanocatalysts

Xiaoping Wang, Huaijun Ma, Donge Wang, Lin Wang, Yiwen Yang, Jianqiang Han, Wei Qu, Lin Yang, Shuaiqi Wang, and Zhijian Tian*



Cite This: *ACS Omega* 2023, 8, 16384–16394



Read Online

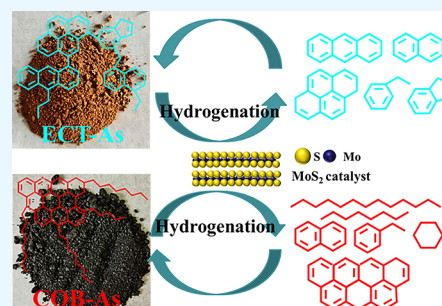
ACCESS |

Metrics & More

Article Recommendations

Supporting Information

ABSTRACT: Asphaltene, the most complex and recalcitrant fraction of heavy oil, was investigated in this study to gain new insights into its structure and reactivity. Two types of asphaltenes, ECT-As and COB-As, were extracted from ethylene cracking tar (ECT) and Canada's oil sands bitumen (COB), respectively, and used as reactants for slurry-phase hydrogenation. Characterization of ECT-As and COB-As was carried out by a combination of techniques, including XRD, elemental analysis, simulated distillation, SEM, TEM, NMR, and FT-IR, to gain insights into their composition and structure. A dispersed MoS₂ nanocatalyst was used to study the reactivity of ECT-As and COB-As under hydrogenation conditions. The results showed that under optimal catalytic conditions, the vacuum residue content of hydrogenation products could be reduced to less than 20%, and the products contained over 50% light components (gasoline and diesel oil), indicating that ECT-As and COB-As were effectively upgraded. The characterization results indicated that ECT-As contained a higher aromatic carbon content, shorter alkyl side chains, fewer heteroatoms, and less highly condensed aromatics than COB-As. The light components (gasoline and diesel oil) of ECT-As hydrogenation products mainly consisted of aromatic compounds with 1–4 rings, with the alkyl chains mainly composed of C1–C2, while light components of COB-As hydrogenation products were mainly composed of aromatic compounds with 1–2 rings and C11–C22 paraffins. The characterization of ECT-As and COB-As and their hydrogenation products revealed that ECT-As was an “archipelago type” asphaltene, composed of multiple small aromatic nuclei interconnected through short alkyl chains, while COB-As was an “island type” asphaltene, with long alkyl chains connected to aromatic nuclei. It is suggested that the structure of asphaltene has a significant impact on both its reactivity and product distribution.



1. INTRODUCTION

With the increasing demands for gasoline and middle distillates as well as the declining supplies of light oil in the last decades, upgrading residue and heavy oil to produce light liquid fuels has attracted great attention from both industrial and academic fields.^{1,2} Slurry-bed hydrogenation is an essential technology to upgrade heavy oil into light liquid fuels.^{3–5} Molybdenum disulfide (MoS₂) with high catalytic activity, sulfur resistance, and poisoning resistance is widely used as the active component of the slurry-bed hydrogenation catalyst for upgrading heavy oil. MoS₂ with few layers and short slabs can expose more active sites and thus improve the catalytic activity of MoS₂.^{6,7} Lee et al. synthesized a nanosized MoS₂ catalyst that achieved a liquid oil yield of over 90% in the hydrogenation of vacuum residues.⁸ Smith and Tye found that an exfoliated MoS₂ catalyst with few layers displayed notable catalytic activity for the hydrogenation of Cold Lake bitumen.⁹ A quasi-single-layer MoS₂ nanocatalyst developed by our group also exhibited excellent catalytic hydrogenation performance of heavy oils in a batch reactor.¹⁰ More recently, Pan et al.¹¹ achieved a one-pass conversion of 65 wt % and a liquid oil

yield of 93 wt % for vacuum residue (VR) hydrogenation using Mo single-atom catalysts.

By solvent extraction and adsorption chromatography, heavy oil is fractionated into four components: saturates, aromatics, resins, and asphaltenes, also called as SARA fractions. Asphaltene is the fraction of crude oil that is insoluble in paraffin solvents such as *n*-pentane, *n*-hexane, or *n*-heptane but soluble in aromatic solvents such as benzene and toluene.^{12,13} Asphaltene has considerable practical significance in the heavy oil hydrogenation process since it hinders the activity and life of hydrogenation catalysts. Asphaltene is the most recalcitrant and complex component of heavy oil and is regarded as the primary coke precursor in heavy oil conversion.^{14–16} Therefore, the catalytic hydrogenation of asphaltene is a vital process that needs to be studied in detail. The hydrogenation reactivity

Received: February 21, 2023

Accepted: April 13, 2023

Published: April 26, 2023



of asphaltene depends on its structure.¹⁷ Thus, the molecular structure of asphaltene has been the subject of numerous studies.^{18–21} And different analysis techniques,^{22–24} including X-ray powder diffraction (XRD), elemental analysis, simulated distillation, scanning electron microscopy (SEM), transmission electron microscopy (TEM), nuclear magnetic resonance (NMR), Fourier transform infrared (FT-IR), and gas chromatography–mass spectrometry (GC–MS), are applied to reveal some valuable descriptions of the chemical compositions and structures of asphaltene.

There are still some debates on the molecular structure unit of asphaltene. Nonetheless, it is indisputable that the structural unit of asphaltene consists of aromatic core and alkyl side chains and may also contain heteroatoms or metals.^{25,26} Asphaltene molecular structure units are classified into three types, namely, “island type”, “archipelago type”, and “hybrid type” (“island type” and “archipelago type” exist at the same time). “Island type”¹⁹ means that the asphaltene molecular structure unit is made up of only one fused aromatic ring as the center that is surrounded by several cycloalkyl rings, short linear alkyl groups, and side chains containing heteroatoms. “Archipelago type”²⁷ represents that the asphaltene molecular structural unit contains several structures similar to “island type”. Asphaltene structural units are connected through alkyl chains with or without heteroatoms. “Hybrid type”²⁸ refers to the asphaltene molecular structure unit containing both “island type” and “archipelago type”, and there is no relevant quantitative report on the proportion of the two models.

The properties of asphaltenes are mainly determined by heavy oil, and the properties of heavy oil from different sources vary greatly.¹⁷ The heavy oil in the refinery mainly comes from crude oil and secondary heavy oil generated during the petroleum refining process. Ethylene cracking tar (ECT), also known as ethylene tar, is a kind of typical secondary heavy oil. ECT is a byproduct of naphtha steam cracking to ethylene unit and a product of high-temperature polycondensation of initial cracking raw materials during the reaction process. ECT has the characteristics of short side chain, high aromatic content, high hydrocarbon ratio, low ash, and heavy metal content.²⁹ Canada’s oil sands bitumen (COB) is a kind of natural asphalt, which is obtained from the oil sands in Canada by thermal processing or mining. COB, which falls in the low-API range (<10°), has a high content of sulfur, nitrogen, and metal. COB is composed of hydrocarbon molecules with small amounts of sulfur, nitrogen, oxygen, and metals such as vanadium and nickel.³⁰

In this work, two asphaltenes, ECT-As and COB-As, extracted from representative heavy oils (ECT and COB) were selected for research. The relationship between the asphaltene structure and its hydrogenation reactivity catalyzed by the prepared nano-MoS₂ was studied. The structures of ECT-As and COB-As were characterized by applying XRD, elemental analysis, simulated distillation, SEM, TEM, NMR, and FT-IR. ECT-As and COB-As were utilized as the feedstocks of slurry-phase hydrogenation. A high-pressure reactor was used for catalytic hydrogenation of ECT-As and COB-As. Then, the hydrogenation products of ECT-As and COB-As were characterized by simulated distillation and GC–MS.

2. EXPERIMENTAL SECTION

2.1. Materials. The compositions of ECT and COB are shown in Table 1. Asphaltenes were extracted based on the

Table 1. Compositions of ECT and COB

components	ECT	COB
C, wt %	91.8	81.7
H, wt %	6.9	9.1
N, wt %	0.2	0.9
S, wt %	0.5	5.7
O, wt % ^a	0.6	2.6
H/C atomic ratio	0.9	1.3
<180 °C, GO, wt %	0	0
180–350 °C, DO, wt %	40.8	0
350–560 °C, VGO, wt %	30.3	15.5
>560 °C, VR, wt %	28.9	84.5

^aThe content of the oxygen element is obtained by difference.

ASTM D-3279 method. *n*-Heptane (210 g) and crude oil (70 g) were added to the ground flask, and the mixture was stirred for 1 h. The insoluble precipitations were obtained by removing the oil solution of *n*-heptane with a Büchner funnel. The insoluble precipitations were then washed with *n*-heptane in the Soxhlet extractor until the reflux was colorless, and then dried in a vacuum oven at 110 °C for 12 h. Asphaltenes isolated from COB and ECT were named COB-As and ECT-As, respectively. The compositions of ECT-As and COB-As are listed in Table 2. *n*-Heptane (C₇H₁₆, 99.5%) was supplied from Xilong Chemical Co., Ltd.

Table 2. Compositions of ECT-As and COB-As

components	ECT-As	COB-As
C, wt %	92.4	80.7
H, wt %	6.7	8.1
N, wt %	0.2	1.3
S, wt %	0.5	7.4
O, wt % ^a	0.2	2.5
H/C atomic ratio	0.9	1.2
<180 °C, GO, wt %	0	0
180–350 °C, DO, wt %	0	0
350–560 °C, VGO, wt %	18.2	4.9
>560 °C, VR, wt %	81.8	95.1

^aThe content of the oxygen element is obtained by difference.

2.2. Characterization of ECT-As and COB-As. The X-ray powder diffraction (XRD) spectra were collected by a PANalytical X’Pert Pro X-ray diffractometer. The XRD was operated at 40 mA and 40 kV using nickel-filtered Cu K_α radiation ($\lambda = 1.5418 \text{ \AA}$) with 2θ ranging from 5 to 70°. The Raman spectrum was collected by the Nano Wizard Ultra Speed&inVia Raman-Atomic Force Microscope. The morphologies and sizes of COB-As and ECT-As were collected by FESEM (JSM-7800F). HRTEM images were obtained with a JEM 2100F microscope. A Thermo Scientific FLASH 2000 organic elemental analyzer was used to analyze the CHNS elemental of COB-As and ECT-As. SIMDIS was operated at Agilent 7890B equipped with an HP-5 column (30 m long, 0.25 mm diameter), according to the ASTM D7169 standard test method. The FT-IR spectra were obtained with a NICOLET Is50 spectrometer operated at 64 scans at a spectral resolution of 4 cm⁻¹. Asphaltene/KBr mixture samples (0.5% (w/w)) were prepared by using spectroscopic grade KBr. The ¹³C and ¹H NMR spectra of asphaltenes were recorded on a Bruker AVANCE III HD spectrometer at 700 MHz for protons. Deuterated chloroform (*d*-chloroform) and

tetramethylsilane (TMS) were used as the solvent and internal calibration standard, respectively.

The molecular parameters, including the fraction of aromatic carbon (f_a), the average number of carbons per alkyl side chain (n), the percentage of the substitution of aromatic rings (σ), and the condensation degree of the aromatic ring (H_{AU}/C_A), were calculated by the following formulas according to the results of NMR spectroscopy:^{31–33}

$$f_a = \frac{C_{ar}}{C_{ar} + C_{al}} \quad (1)$$

$$n = \frac{H_\alpha + H_\beta + H_\gamma}{H_\alpha} \quad (2)$$

$$\sigma = \frac{H_\alpha/2}{H_\alpha/2 + H_A} \quad (3)$$

$$H_{AU}/C_A = \frac{H_A + H_\alpha/2}{C/H - (H_\alpha/2 + H_\beta/2 + H_\gamma/3)} \quad (4)$$

Here, C_{ar} is the content of aromatic carbon, and C_{al} is the content of aliphatic carbon. H_A , H_α , H_β , and H_γ are the content of aromatic hydrogen, hydrogen in saturated groups α to aromatic rings, hydrogen in saturated groups β to aromatic rings, and hydrogen in saturated groups γ or further to aromatic rings, respectively. C/H is the molar ratio of carbon to hydrogen measured by the organic element analyzer.

2.3. Hydrogenation Reaction of COB-As and ECT-As. An intercalated-layer MoS_2 nanocatalyst with few layers and short slab length was synthesized by the hydrothermal method with L-cysteine and molybdenum trioxide as S and Mo precursors for the catalytic hydrogenation of asphaltene. The preparation and characterization of the MoS_2 nanocatalyst are detailed in the [Supporting Information](#). The hydrogenation reactions of ECT-As and COB-As were conducted in a 100 mL high-pressure reactor. For ECT-As or COB-As hydrogenation, 30.0 g of ECT-As or COB-As and 0.3 g of the MoS_2 catalyst were put into the autoclave. The air in the batch microreactor was replaced with hydrogen at 0.5–1.5 MPa three times, and then the reactor was filled with hydrogen at 15–17 MPa at room temperature. Catalytic hydrogenation reactions were conducted at 405–420 °C for 2–8 h with mechanical stirring at 300 rpm. After the autoclave cooled to room temperature naturally, the hydrogenation products were collected manually. Hydrogenation products of ECT-As were dominated as liquid with a small amount of gas, while hydrogenation products of COB-As were liquid, separated asphaltene, and a small amount of gas. An Agilent 7890 gas chromatograph equipped with a thermal conductivity detector and hydrogen flame ion detector, four switching valves, and six chromatographic columns, including one HP-AL/S capillary column (30 m \times 0.53 mm \times 15 mm), one 5A molecular sieve column (0.15 m \times 0.26 mm \times 2.1 mm), and four Porapak Q columns (0.15 m \times 0.26 mm \times 2.1 mm), was used to analyze the gas products. The liquid and asphaltene product distributions were measured by simulated distillation (denoted as SIMDIS) according to the standard test method of ASTM D7169. The samples were fractionated into four fractions based on boiling temperature (b.t.): gasoline oil (GO, b.t. < 180 °C), diesel oil (DO, 180 °C < b.t. < 350 °C), vacuum gas oil (VGO, 350 °C < b.t. < 560 °C), and vacuum residues (VR, b.t. > 560 °C). The GO fraction and DO fraction were separated from the

liquid products by distillation and then qualitatively analyzed in an Agilent 7890B-5977A GC–MS equipped with an HP-5 column (30 m long, 0.25 mm diameter).

The following equations were used to calculate liquid yield, separated asphaltene yield, and VR conversion:

$$\text{Liquid yield (\%)} = W_{\text{liquid}}/W_{\text{feed}} \times 100 \quad (5)$$

$$\text{Asphaltene yield (\%)} = W_{\text{asphaltene}}/W_{\text{feed}} \times 100 \quad (6)$$

where W_{liquid} , $W_{\text{asphaltene}}$, and W_{feed} are the mass of liquid, asphaltene, and feed, respectively.

$$\begin{aligned} \text{VR conversion (\%)} \\ = (W_{\text{VR of feed}} - W_{\text{VR of product}}) \times 100 / (W_{\text{VR of feed}}) \end{aligned} \quad (7)$$

where $W_{\text{VR of feed}}$ and $W_{\text{VR of product}}$ are the VR mass of the feed and product, respectively.

The normalized GO, DO, VGO, and VR contents of COB-As hydrogenation products were calculated according to the following formulas:

$$\begin{aligned} \text{Normalized GO content (\%)} \\ = (W_{\text{GO of liquid}} + W_{\text{GO of asphaltene}}) \times 100 / (W_{\text{feed}}) \end{aligned} \quad (8)$$

where $W_{\text{GO of liquid}}$ is the GO mass of the liquid and $W_{\text{GO of asphaltene}}$ is the GO mass of the asphaltene. The normalized DO, VGO, and VR contents were calculated in the same way as normalized GO.

3. RESULTS AND DISCUSSION

3.1. Characterization of ECT-As and COB-As. The elemental analysis and the SIMDIS analysis results of ECT and COB are listed in [Table 1](#). According to [Table 1](#), ECT contains a lower H/C molar ratio than COB, indicating that the unsaturation degree of COB is lower than that of ECT. In addition, COB contains higher contents of N and S than ECT, because COB comes from crude oil, while raw materials for ECT generation are refined. The SIMDIS curves of ECT and COB are shown in [Figure S4](#). VR is the dominant component in COB, but DO and VGO are the major components in ECT, indicating that COB has higher boiling point components than ECT. No GO component was detected in both ECT and COB. The nature and composition of COB and ECT are different, which is attributed to the fact that COB is formed through a long-term geological process, while ECT is formed from rapid condensation of ethylene during the high-temperature cracking reaction.

The SIMDIS analysis and the elemental analysis results of asphaltene from ethylene cracking tar (ECT-As) and asphaltene from Canada's oil sands bitumen (COB-As) are listed in [Table 2](#). And the SIMDIS curves of ECT-As and COB-As are shown in [Figure S5](#). As shown in [Table 2](#) and [Figure S5](#), VR is the dominant component in both ECT-As and COB-As; neither GO nor DO was detected in both ECT-As and COB-As. And the contents of VGO in ECT-As and COB-As are 15.5 and 4.9%, respectively. COB-As contains higher contents of heteroatoms (N and S) than ECT-As, particularly sulfur content. Furthermore, ECT-As has a lower H/C ratio than COB-As, implying that ECT-As has a higher aromatic degree than COB-As. Accordingly, ECT-As and COB-As mainly contain heavy components.

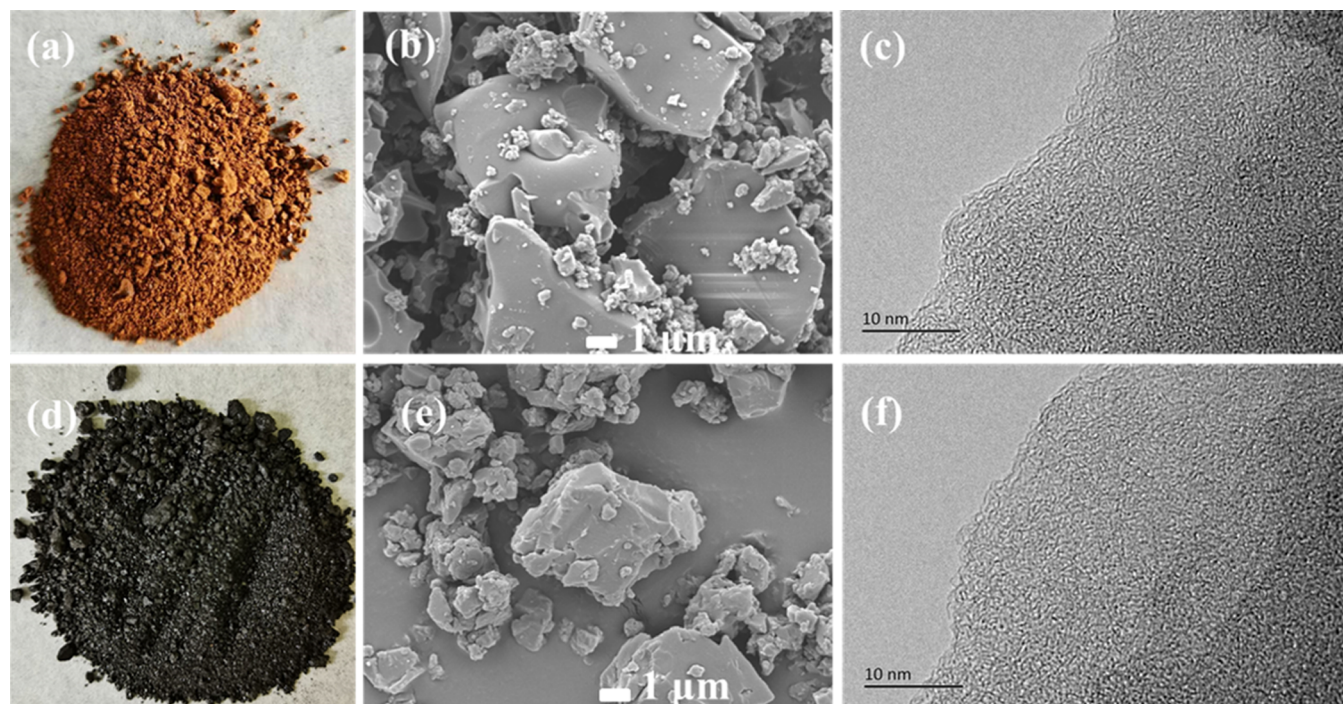


Figure 1. (a) Photograph, (b) SEM image, and (c) HRTEM image of asphaltene of ethylene cracking tar (ECT-As); (d) photograph, (e) SEM image, and (f) HRTEM image of asphaltene of Canada's oil sands bitumen (COB-As).

The obtained ECT-As and COB-As are orange powder and black powder, respectively (Figure 1a,d). SEM and TEM were further applied to characterize the microscopic morphology of ECT-As and COB-As. It is shown that the agglomerate particles of ECT-As are similar to those of COB-As, ranging from hundreds of nanometers to several microns (Figure 1b,e). Both agglomerate particles of ECT-As and COB-As are smooth blocks with irregular particles on the surface, which is due to the aggregation of asphaltene during precipitation.³⁴ Figure 1c,f shows the HRTEM images of ECT-As and COB-As, respectively. There are no obvious well-ordered graphite-like structures within ECT-As and COB-As according to the HRTEM images. Although ECT-As and COB-As have apparent differences in color, there is no significant difference between them from micromorphology.

Figure 2 shows the XRD patterns of ECT-As and COB-As. The XRD pattern of COB-As shows weak diffraction peaks located at $2\theta = 19$ and 24° , corresponding to the γ and (002) lattice planes of graphite, respectively. In the XRD pattern of

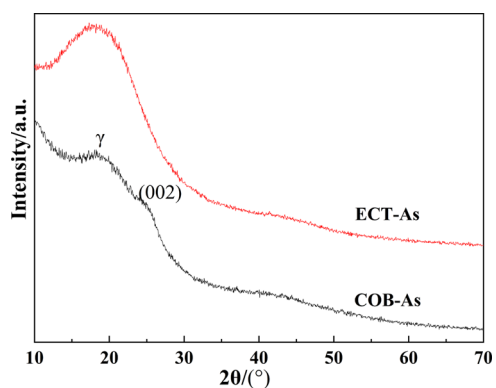


Figure 2. XRD patterns of ECT-As and COB-As.

ECT-As, there is one broad peak ranging from $2\theta = 13$ to 30° with the center at $2\theta = 18^\circ$, indicating the low short-range order of ECT-As. The diffraction peak of the (002) lattice plane of graphite generally originates from the layered aromatic structure, and the diffraction peak of the γ lattice plane originates from the structure of the saturated part (including cycloalkanes and alkanes) of asphaltene.²¹ The narrower and higher the peak of the (002) lattice plane, the higher the graphitization degree of asphaltene is.³⁵ The XRD patterns of ECT-As and COB-As show that the graphitization degree of COB-As is higher than that of ECT-As.

FT-IR was further used to characterize the molecular structure of ECT-As and COB-As. The attribution of absorption peaks in the infrared spectra is listed in Table S1 according to the literature.¹⁷

As shown in Figure 3a, the strong peaks at 3020 and 1602 cm^{-1} are attributed to aromatic C–H stretching vibration and C=C stretching vibration of the skeleton, respectively. Donald et al.³⁶ found that the fairly intense signal of aromatic C–H stretching vibrations suggests that the aromatic rings are sparsely substituted. Therefore, ECT-As is highly aromatized and trace hydrogen of aromatic rings of ECT-As is substituted by alkyl groups. The presence of peaks at 2920, 1455, and 1383 cm^{-1} in Figure 3a shows the existence of methylene ($-\text{CH}_2-$) and methyl ($-\text{CH}_3$) in ECT-As. And the peaks at 812 and 742 cm^{-1} in Figure 6a reflect that ECT-As contains the aromatic ring with di-, tetra-substituted alkyl.

Figure 3b shows the FT-IR spectrum of COB-As. There is a notable peak at 1608 cm^{-1} but a weak peak at 3058 cm^{-1} . Zhu et al.³³ reported that the weak peak at 3058 cm^{-1} can be attributed to a large number of hydrogen on the aromatic rings being replaced by side chain alkyl. It is suggested that COB-As contains highly substituted aromatic rings or the aromatic rings of COB-As are condensed. In addition, the peaks at 2919, 1455, and 1370 cm^{-1} in Figure 6b also indicate that COB-As

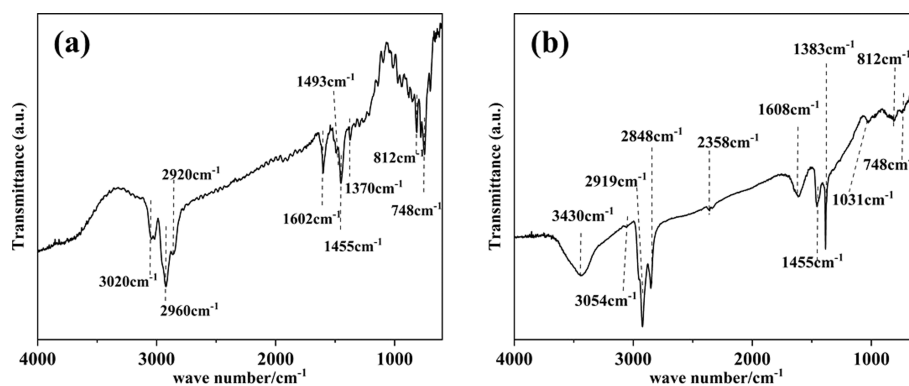


Figure 3. (a) FT-IR spectrum of ECT-As; (b) FT-IR spectrum of COB-As.

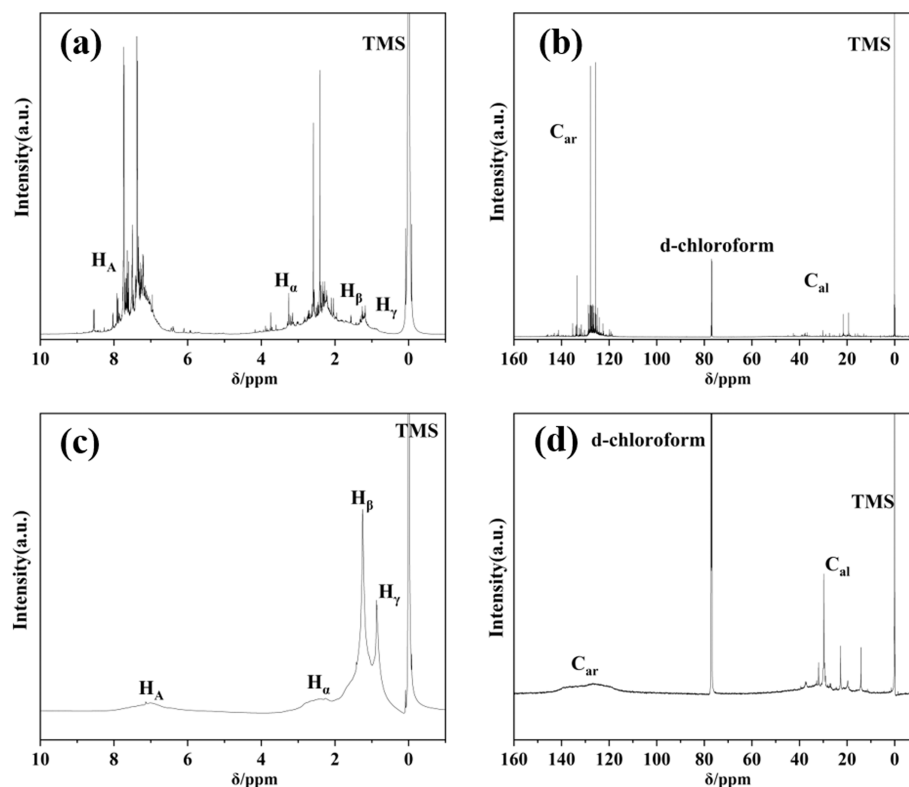


Figure 4. (a) ^1H and (b) ^{13}C NMR spectra of ECT-As; (c) ^1H and (d) ^{13}C NMR spectra of COB-As.

contains methylene ($-\text{CH}_2-$) and methyl ($-\text{CH}_3$). The weak peaks at 812 and 742 cm^{-1} in Figure 3b illustrate that the hydrogen of the aromatic ring of COB-As is highly substituted by alkyl.

The broad peak at 3480 cm^{-1} (between 3600 and 3100 cm^{-1}) in Figure 3b suggests that COB-As contains rich O–H or N–H groups. In addition, according to the high content of nitrogen of the elemental analysis result, the peak located at 3480 cm^{-1} in the spectrum of COB-As is probably related to the N–H functional groups. The weak peak at 1032 cm^{-1} in the FT-IR spectrum of COB-As may be attributed to sulfoxide (S=O) functional groups.

Accordingly, ECT-As and COB-As both contain aromatic rings and alkyl side chains, but the substitution degree of hydrogen on the aromatic ring of ECT-As is lower than that of COB-As. In addition, COB-As contains N–H and S=O groups.

NMR is a powerful approach to elucidate the chemical structures of asphaltenes. Figure 4 demonstrates the ^1H and ^{13}C spectra of two asphaltenes of ethylene cracking tar (ECT-As) and Canada's oil sands bitumen (COB-As). The assignments of ^1H and ^{13}C NMR of ECT-As and COB-As are summarized in Table 3. The ^1H NMR spectrum was divided into four regions: H_A (6.0–9.0 ppm), aromatic hydrogen; H_α (2.0–4.0 ppm), aliphatic hydrogen on carbon α to aromatic rings; H_β (1.0–2.0 ppm), aliphatic hydrogen on carbon β to aromatic rings; and H_γ (0.5–1.0 ppm), aliphatic hydrogen on carbon γ or further to aromatic rings. For the ^{13}C NMR spectrum, there are two characteristic regions, one from 110 to 160 ppm for aromatic carbons (C_ar) and the other from 10 to 60 ppm for aliphatic carbons (C_al). As shown in Figure 4a,c, the resonance peaks in the ^1H spectrum of COB-As are much sharper than those of ECT-As; nevertheless, the peaks in the C_al region of ECT-As are significantly more robust than those in the C_al region. The peak at 77.2 ppm in Figure 4a,c

Table 3. Assignments of ^1H and ^{13}C NMR Resonances and the Calculated Structural Parameters of ECT-As and COB-As³¹

symbol	peak ranges (ppm)	assignment	ECT-As	COB-As
H_γ	0.5–1.0	hydrogen in saturated groups γ or further to aromatic rings	0.03	0.25
H_β	1.0–2.0	hydrogen in saturated groups β to aromatic rings	0.21	0.6
H_α	2.0–4.0	hydrogen in saturated groups α to aromatic rings	0.35	0.09
H_A	6.0–9.0	aromatic protons	0.42	0.06
C_ar	10–60	aromatic carbons	0.94	0.45
C_al	110–160	aliphatic carbons	0.06	0.55
f_a		aromatic carbon fraction	0.94	0.45
σ		ratio of substitution of aromatic rings	0.29	0.44
$\text{H}_\text{AU}/\text{C}_\text{A}$		degree of aromatic ring condensation	0.69	0.29
n		average length of alkyl chains	1.68	10.22

represents the solvent peak of deuterated chloroform (*d*-chloroform).

The relative quantities of H_ar , H_w , H_β , H_γ , C_ar , and C_al and the calculated structural parameters of ECT-As and COB-As are listed in Table 3. The contents of H_w , H_β , and H_γ in ECT-As and COB-As varied. The high content of H_α and H_β in ECT-As implies that the alkyl side chain of ECT-As is mainly short alkyl: α -methyl and β -methyl. Differently, the alkyl side chain in COB-As is dominated by β -methyl and γ -methyl evidenced by the high content of H_β and H_γ . The calculated average numbers of carbons per alkyl side chain (n) of ECT-As and COB-As are 1.68 and 10.22, indicating that COB-As contains longer alkyl chains than ECT-As.

According to Table 3, 42% of the hydrogen in ECT-As is aromatic hydrogen, while only 6% of the hydrogen in COB-As is aromatic hydrogen. ECT-As contain 94% aromatic carbon, but COB-As only have 45% aromatic carbon. It is suggested that carbon in ECT-As mainly exists as aromatic compounds, while half of the carbon in COB-As exists in the form of alkyl substituents. Furthermore, the substitution ratios of aromatic rings (σ) in ECT-As and COB-As are 0.29 and 0.44, respectively, suggesting that the substitution ratio of aromatic rings of ECT-As is lower than that of COB-As, which is consistent with the FT-IR results. The condensation degree of the aromatic ring is described by the $\text{H}_\text{AU}/\text{C}_\text{A}$ value. The higher the $\text{H}_\text{AU}/\text{C}_\text{A}$ value, the lower the condensation degree is.³⁷ The $\text{H}_\text{AU}/\text{C}_\text{A}$ values of ECT-As and COB-As are 0.69 and 0.29, respectively, suggesting that COB-As contains bigger aromatic nuclei than ECT-As.

In summary, ECT-As has a higher aromaticity degree, a lower substitution ratio of aromatic rings, and a lower aromatic condensation degree than COB-As. Therefore, ECT-As consists of low-condensation aromatic nuclei with a small amount of short-chain alkyl. COB-As mainly contains highly condensed aromatic nuclei and long-chain alkanes, and the carbon content occupied by these two structures is basically the same.

Based on the characterization results of ECT-As and COB-As, ECT-As mainly contains highly substituted aromatic with short alkyl chains, but COB-As mainly contains highly condensed aromatic nuclei with long alkyl chains and heteroatoms (N and S). Significant differences can be

observed, such as COB-As has a higher graphitization degree, higher heteroatom content (particularly sulfur), higher content of aromatic carbon, and longer and more alkyl side chain and contains larger aromatic nuclei than ECT-As. The structure and compositions of ECT-As and COB-As are different, attributed to the difference of their raw materials. The difference in the nature of ECT-As and COB-As is expected to affect their hydrogenation activities and product distributions.

3.2. Catalytic Hydrogenation of ECT-As and COB-As.

3.2.1. Catalytic Hydrogenation of ECT-As. The catalytic hydrogenation reactions of ECT-As were carried out to further investigate the relationship between the reactivity and structure of ECT-As. At room temperature, the reactant ECT-As is solid. Applying the synthesized nano- MoS_2 as a catalyst, the hydrogenation products of ECT-As were dominated as liquid with a small amount of gas at room temperature after a 2–8 h reaction. The liquid product yield of ECT-As is higher than 95%, indicating the well upgrading of ECT-As.

The gas products generated by ECT-As were analyzed by GC. As shown in Figure S6, the components of the gas generated during the ECT-As hydrogenation process are mainly methane, ethane or ethene, C3 alkanes or olefins, and a small number of C4–C7 alkanes or olefins. With the extension of the reaction time, the content of all components of the gas increased.

The liquid products of ECT-As were analyzed by simulated distillation. Figure 5 displays the VR conversion and liquid

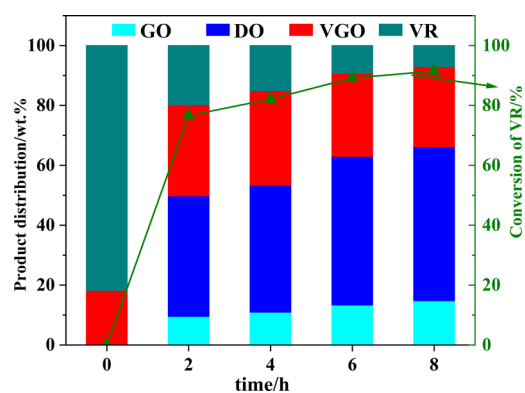
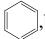
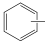
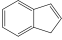
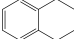


Figure 5. Product distributions and conversion of VR of hydrogenated ECT-As at different reaction times. Reaction conditions for ECT-As: catalyst, 0.3 g; ECT-As, 30.0 g; initial pressure, 15.0 MPa; reaction temperature, 420 °C; time = 2, 4, 6, and 8 h.

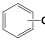
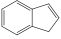
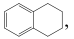
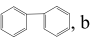
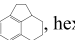
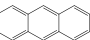
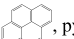
product distribution of ECT-As at different reaction times. From 0 to 8 h, the content of GO and DO increased to 14.8 and 31.5%, respectively; meanwhile, the content of VR decreased from 81.8 to 7.1%. The content of VGO increased from 18.2 to 30.5% over 6 h and then decreased to 26.7% at 8 h. From 0 to 2 h, the conversion of VR rapidly reached to 76.6%, indicating that VR is rapidly converted to VGO, DO, or GO. With the reaction time further increasing to 8 h, the VR conversion slowly increased to 91.5%, suggesting that VR is slowly converted to GO, DO, or VGO. Furthermore, it is suggested that small aromatics in ECT-As are easy to be converted into light components, and the components that are difficult to convert are probably highly condensed aromatics. Thus, the light components in ECT-As products were further studied in detail.

Table 4. Content of Main Components in ECT-As-G and COB-As-G^a

Components	Content in ECT-As-G (wt%)	Content in COB-As-G(wt%)
 ,benzene	1.2	5.3
 -C _n ,n=1-5,alkylbenzene	53.9	24.3
 ,indene	15.7	0
 ,tetralin	19.4	2.0
C _n H _{2n+2} ,paraffins	3.9(n=6,7)	51.7(n=5-13)
C _n H _{2n} ,cycloparaffins	5.9(n=5-9)	16.4(n=5-11)

^aReaction conditions for ECT-As-G: catalyst, 0.3 g; ECT-As, 30.0 g; initial pressure, 15.0 MPa; reaction temperature, 420 °C; *t* = 8 h. Reaction conditions for COB-As-G: catalyst, 0.3 g; COB-As, 30.0 g; initial pressure, 17.0 MPa; reaction temperature, 405 °C; *t* = 6 h. ECT-As-G and COB-As-G are the GO fractions of ECT-As and COB-As liquid products, respectively.

Table 5. Content of the Main Component in ECT-As-D and COB-As-D^a

Components	Content in ECT-As-D (wt%)	Content in COB-As-D(wt%)
 -C _n ,n=3-6, alkylbenzene	6.9	12.9
 , indene	8.8	6.1
 , tetralin	35.2	36.4
 , biphenyl	11.0	3.5
 , hexahydrofluorene	5.9	0
 , anthracene	21.6	5.2
 , pyrene	4.5	0
C _n H _{2n+2} , paraffins	0	35.9(n=11-22)

^aReaction conditions for ECT-As-D: catalyst, 0.3 g; ECT-As, 30.0 g; initial pressure, 15.0 MPa; reaction temperature, 420 °C; *t* = 8 h. Reaction conditions for COB-As: catalyst, 0.3 g; COB-As, 30.0 g; initial pressure, 17.0 MPa; reaction temperature, 405 °C; *t* = 6 h. ECT-As-D and COB-As-D are the DO fractions of ECT-As and COB-As liquid products, respectively.

GC–MS was applied to identify the detailed components of the gasoline and diesel fractions of the liquid product of ECT-As after an 8 h hydrogenation reaction. The gasoline and diesel fractions in the hydrogenation products of ECT-As were named as ECT-As-G and ECT-As-D. As shown in Figure S7, about 100 substances were detected in the GC spectra of ECT-As-G and ECT-As-D. We classify them and list them in Tables 4 and 5, respectively.

As shown in Table 4 and Figure S7, ECT-As-G is rich in monoaromatic hydrocarbons, especially benzenes with C2–C4 alkyl groups. ECT-As-G also contains 35.1% diaromatic hydrocarbons, such as indene and tetralin. The total content of aromatics in ECT-As-G is 90.2%. In addition, ECT-As-G also contains 5.9% cycloalkanes (C5–C9) and 3.9% paraffins (C6–C7). Therefore, ECT-As-G mainly contains C7–C11 alkylbenzene, indene, and tetralin.

As shown in Table 5 and Figure S7, the main compounds detected in ECT-As-D are bi- and triaromatic hydrocarbons, including indene, tetralin, biphenyl, anthracene, and hexahydrofluorene. A small number of tetra-aromatic hydrocarbons (pyrene) and monoaromatic hydrocarbons (C9–C12 alkylbenzene) were also detected in ECT-As-D. The total content of aromatics in ECT-As-D is 100%. Therefore, ECT-As-D mainly contains aromatic compounds with 1–4 rings.

The mass fraction of GO fraction in liquid products is 14.8%, and the GO fraction contains 3.9% paraffins, so the mass fraction of paraffins in liquid products is 0.6%. And the yield of the liquid produced by the reaction of ECT-As is 98%, so ECT-As contains 0.6% paraffins (C6–C7). It is suggested that almost all compounds in ECT-As are aromatics, which is consistent with the results of NMR. In addition, the gas products are mainly methane, ethane, and ethylene, with only a small amount of C4–C7 alkanes or olefins. And according to

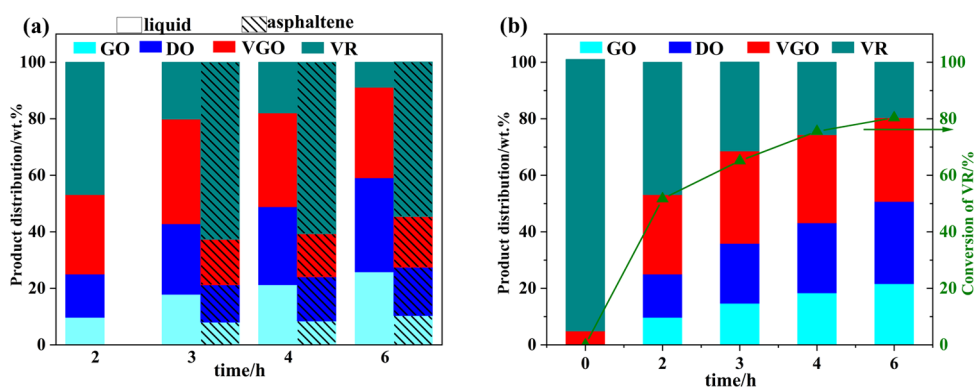


Figure 6. (a) Product distributions of liquid and precipitated asphaltene during COB-As catalytic hydrogenation; (b) product distributions and total conversion of VR of COB-As at different reaction times. Reaction conditions for COB-As: COB-As, 30.0 g; initial pressure, 17.0 MPa; reaction temperature, 405 °C; time = 2, 3, 4, and 6 h.

the NMR result, the average number of carbons per alkyl side chain (n) of ECT-As is 1.68. Therefore, the alkyl chain of ECT-As is mainly short alkyl (C1–C2).

To sum up, solid ECT-As mainly generate liquid with a small amount of gas under the catalytic hydrogenation of the MoS₂ nanocatalyst. The liquid yield was 98% and the total content of GO and DO was 66.3% after the reaction at 420 °C for 8 h, which indicates that ECT-As has achieved good upgrading under the catalysis of MoS₂. The characterization of the light components (GO and DO) of the ECT-As liquid product shows that the light components of the ECT-As liquid product are mainly aromatic compounds with 1–4 rings, and the alkyl chain of ECT is mainly C1–C2 alkyl.

3.2.2. Catalytic Hydrogenation of COB-As. Similarly, catalytic hydrogenation of COB-As was used to further study the relationship between reactivity and structure of COB-As. At room temperature, the reactant COB-As is solid. The product obtained by hydrogenation of solid COB-As for 2 h is a viscous liquid and a small amount of gas at room temperature. Further extending the reaction time to 3 h, the viscosity of the liquid is significantly reduced, and obvious phase separation occurs. And part of asphaltene is separated from the product during COB-As hydrogenation progress. Speight³⁸ found that asphaltene is easy to form aggregates in weakly polar solvents, indicating that the polarity of the liquid products of COB-As is weak. For further hydrogenation, although the gas yield is less than 4%, there is always phase separation of liquid and asphaltene. And the yield of liquid is about 72% and the yield of asphaltene is about 24%. It shows that COB-As has achieved upgrading under the catalysis of the MoS₂ nanocatalyst.

GC was used to analyze the gas products of COB-As. As shown in Figure S8, the composition of the gas produced by COB-As cracking is consistent with that of the gas produced by ECT-As cracking, and the reaction law of each component varies with the reaction time that is also consistent.

Distillation range analysis of liquid and asphaltene produced by hydrogenation of COB-As was carried out by simulated distillation. Figure 6 shows the product distribution of the liquid and asphaltene and the total VR conversion and product distribution of hydrogenated COB-As at different reaction times.

The product distributions of liquid and asphaltene of hydrogenated COB-As with 2–6 h are shown in Figure 6a. From 2 to 6 h, the GO and DO content of liquid products

increased to 25.8 and 33.3%, respectively; meanwhile, the VR content decreased to 8.8%, and the VGO content first increased to 37.1% over 4 h and then decreased to 32.0% at 6 h. With the reaction time increasing from 3 to 6 h, the VR content in asphaltene produced by COB-As hydrogenation gradually decreased from 62.7 to 54.7%, the VGO content increased from 16.1 to 18.0%, and the GO and DO content increased from 8.0 to 10.4 and 13.2 to 17.1%, respectively. The conversion of VR and VGO in asphaltene is slower than that in liquid, probably because asphaltene does not have good contact with the MoS₂ catalyst. The simulated distillation results of asphaltene show that the asphaltene produced in the reaction process is also the product of COB-As upgrading. Therefore, the total simulated distillation results of liquid and asphaltene can reflect the actual composition of the hydrogenation products of COB-As.

Figure 6b shows the VR conversion and the product distribution of hydrogenation products of COB-As at different reaction times. With the reaction time increasing from 0 to 6 h, the GO and DO content increased to 21.7 and 29.1%, respectively, and the VR content decreased from 95.1 to 19.6%. The VGO content increased from 4.9 to 32.7% over 4 h and then decreased to 29.6% at 6 h, indicating that under the catalysis of MoS₂, the VR fraction was converted into VGO, DO, or GO fraction, and the VGO fraction was further converted into DO or GO fraction.

GC–MS was used to further identify the detailed composition of GO and DO fractions of the liquid of COB-As hydrogenated for 6 h. The GO and DO fractions of COB-As liquid are named as COB-As-G and COB-As-D, respectively.

As shown in Figure S9, about 100 substances were identified in the GC spectra of COB-As-D and COB-As-G. We also classify them and list them in Tables 4 and 5, respectively. As shown in Table 4 and Figure S9, 51.7% C5–C13 paraffins were detected in COB-As-G, with the highest content of heptane. COB-As-G also contains C5–C11 cycloalkane, of which cyclopentane is the highest. In addition, COB-As-G also contains 29.6% monoaromatic hydrocarbons, such as benzene with C1–C5 alkyl groups. Therefore, COB-As-G is mainly composed of paraffins (C5–C13), C7–C11 alkylbenzene, and cycloalkanes (C5–C11).

As shown in Table 5 and Figure S9, the aromatics contained in COB-As-D are mainly diaromatic and monoaromatic hydrocarbons, such as indene, tetralin, biphenyl, and C9–

C12 alkylbenzene. C11–C22 paraffins were also detected in COB-As-G, with the highest content of C15. The total contents of aromatics and paraffins in COB-As-D are 64.1 and 35.9%, respectively. Therefore, COB-As-D is mainly composed of aromatic compounds with 1–2 rings and C11–C22 paraffins.

The mass fractions of GO and DO fractions in liquid products are 25.8 and 33.3%, respectively. And the mass fractions of paraffins in GO and DO are 51.7 and 35.9%, respectively, so the content of paraffins in liquid products is higher than 25.3%. Furthermore, the yield of liquid products is 71.6%, so COB-As contains at least 18.1% paraffins (C5–C22), which is consistent with the NMR results. Moreover, the average length of the COB-As alkyl side chain is 10.22 according to the results of NMR. Therefore, COB-As contains not less than 18.1% long-chain alkanes (C5–C22).

In summary, solid COB-As generates liquid, asphaltene, and a small amount of gas under optimal reaction conditions with a nano-MoS₂ catalyst. The total yield of liquid and asphaltene is 97%, and the total content of GO and DO is 50.8%, indicating good upgrading of COB-As under the catalysis of MoS₂. The characterization of light components (GO and DO) of COB-As hydrogenation products shows that the light components of COB-As hydrogenation products are aromatic compounds with 1–2 rings and C5–C22 paraffins.

3.2.3. Relationships between the Structure and Reactivity of ECT-As and COB-As. Compared with raw materials, the VR content of hydrogenation products under optimal catalytic conditions can be reduced to less than 20% and hydrogenation products contain more than 50% light components (GO and DO), indicating that ECT-As and COB-As both have achieved well upgrading. It is suggested that the MoS₂ nanocatalyst has excellent catalytic hydrogenation activity for both ECT-As and COB-As. Zheng et al.¹⁰ reported that highly dispersed nano-MoS₂ catalysts can contact with asphaltenes completely, thus rapidly converting them into light components through catalytic hydrogenation and cracking reactions. Therefore, the dispersed MoS₂ nanocatalyst used in this study displays excellent catalytic hydrogenation and depolymerization performance for ECT-As and COB-As.

Although COB-As and ECT-As undergo the same reaction under the catalysis of MoS₂, their products are quite different, which is determined by their structure.¹⁷ Du et al.³⁹ found that heavy oil slurry-bed hydrocracking followed the free radical mechanism. In the presence of dispersed catalysts, the concentration of hydrogen radicals is high, which can promote the cracking of aromatics and cycloalkane. Seki et al.⁴⁰ found that C–C bonds are easily broken and alkyl chains are cracked during the catalytic hydrogenation process at reaction temperatures of higher than 400 °C. The products of ECT-As include partially hydrogenated aromatics such as tetralin and hexahydrofluorene, while only a small amount of pure cycloalkanes, indicating that the aromatics contained in ECT-As have undergone the partial hydrogenation reaction because high reaction temperature is not conducive to complete hydrogenation.⁴¹ And the products of ECT-As only contain 0.8% paraffins but contain a large amount of alkyl benzene, which indicates that the alkyl side chain of ECT-As undergoes the alkyl chain breaking reaction during the hydrogenation reaction, leading to the cracking of aromatic nuclei to produce aromatic compounds with 1–4 rings. Thus, ECT-As mainly undergo aromatic ring hydrogenation and fracture of the alkyl bridge between the aromatic nucleus and the aromatic nucleus

with a MoS₂ nanocatalyst. Furthermore, most of the hydrogen on the ECT-As aromatic ring is not replaced and the alkyl chain of ECT-As is mainly C1–C2 alkyl. Hence, aromatic nuclei in ECT-As must be connected with each other through short alkyl chains. Therefore, ECT-As is composed of several interconnected small aromatic nuclei with short alkyl chains. In other words, ECT-As is an “archipelago type” asphaltene.

According to Ancheyta,¹⁷ dealkylation of the alkyl side chain attached aromatic nuclei of asphaltene results in asphaltene separated from the hydrogenation product due to the different polarities of asphaltene and alkyl side chains. Therefore, the asphaltene separated from the hydrogenation products of COB-As indicates that the dealkylation reaction occurs in the hydrogenation of COB-As. And the liquid hydrogenation products of COB-As are 1–2 rings of aromatic compounds and paraffins from C5 to C22. Therefore, in the hydrogenation catalytic process of COB-As, as in ECT-As, dealkylation and aromatic ring cracking reactions mainly occur. There are also some cycloalkanes in the hydrogenation products, which may be produced by partial hydrogenation of aromatics. Meanwhile, COB-As has large and highly condensed aromatic nuclei and the degree of substitution of the aromatic ring is 0.44, and COB-As contains not less than 18.1% long paraffins, so the long paraffins must connect to the large aromatic nuclei. In addition, COB-As contains N and S heteroatoms, and the infrared spectrum also shows N–H and S=O groups. Therefore, there may be a small amount of alkyl side chains connected with the aromatic nuclei through N–H and S=O groups. It is suggested that COB-As mainly consists of highly condensed aromatic nuclei with long alkyl chains and heteroatoms, which is consistent with the description of the “island type” asphaltene of Mullins.²⁰ That is, COB-As is an “island type” asphaltene.

Catalytic hydrogenation of different asphaltenes requires different reaction conditions. ECT-As is an “archipelago type” asphaltene with multiple small aromatic nuclei and short alkyl chains, while COB-As is an “island type” asphaltene with large aromatic nuclei and long alkyl chains. ECT-As is relatively easy to hydrocrack at high temperatures because ECT-As is formed by condensation at high temperatures and the degree of polycondensation is limited. And it will not be further polycondensation at high temperatures as the alkyl side chain is easy to break. Therefore, “archipelago type” asphaltene like ECT-As can be rapidly cracked to produce light fuel under high reaction temperatures. Differently, the side alkyl chain of the original “island type” asphaltenes like COB-As is easy to crack rapidly at the high reaction temperature, resulting in the phase separation of asphaltene and hydrogenation products due to the large difference in polarity. The separated asphaltene is difficult to be converted into light fuel, as the contact between asphaltene and the catalyst is rather poor. Therefore, in the hydrogenation process of asphaltenes like COB-As, aromatic solvent (benzene and tetralin) or highly aromatic crude oil like ECT can be added to the reaction raw materials to facilitate the contact between asphaltene and the catalyst to obtain more hydrogenation products.

4. CONCLUSIONS

Two representative asphaltenes, ECT-As and COB-As, were extracted as the reactant directly. A dispersed MoS₂ nanocatalyst for the catalytic hydrogenation of ECT-As and COB-As has been synthesized by the hydrothermal method. The catalytic hydrogenation reaction results show that the yield of

liquid products of ECT-As in the hydrogenation reaction at 420 °C for 8 h is 98% and the total mass fraction of GO and DO in liquid products is 66%. And the total yield of liquid and separated asphaltene of the COB-As hydrogenation reaction at 405 °C for 6 h is 97%, and the total mass fraction of GO and DO in products of COB-As hydrogenation is 51%. The results of catalytic hydrogenation show that MoS₂ with a small size and few layers has excellent catalytic performance for the conversion of asphaltene into light liquid fuels. The characterization results show that ECT-As possesses a higher aromatic carbon content, shorter alkyl side chains, fewer contents of heteroatoms, and less highly condensed aromatics than COB-As. Light components (GO and DO) of ECT-As hydrogenation products are mainly aromatic compounds with 1–4 rings, and the alkyl chain of ECT-As is mainly C1–C2 alkyl, and light components of COB-As hydrogenation products are mainly composed of aromatic compounds with 1–2 rings and C11–C22 paraffins. Characterizations of ECT-As and COB-As and their hydrogenation products show that the structure of ECT-As is “archipelago type” and the structure of COB-As is “island type”. The catalytic hydrogenation of “island type” asphaltene requires appropriate solvents and highly active catalysts, while the catalytic hydrogenation of “archipelago type” asphaltene needs high reaction temperatures to crack the asphaltene rapidly and obtain light fuels.

■ ASSOCIATED CONTENT

SI Supporting Information

The Supporting Information is available free of charge at <https://pubs.acs.org/doi/10.1021/acsomega.3c01174>.

Synthesis and characterization of MoS₂ catalysts; SIMDIS and FT-IR of ECT-As and COB-As; and catalytic hydrogenation results of ECT-As and COB-As (PDF)

■ AUTHOR INFORMATION

Corresponding Author

Zhijian Tian – State Key Laboratory of Catalysis, Dalian National Laboratory for Clean Energy, Dalian Institute of Chemical Physics, Chinese Academy of Sciences, Dalian 116023, P.R. China; orcid.org/0000-0002-6092-485X; Email: tianz@dicp.ac.cn

Authors

Xiaoping Wang – State Key Laboratory of Catalysis, Dalian National Laboratory for Clean Energy, Dalian Institute of Chemical Physics, Chinese Academy of Sciences, Dalian 116023, P.R. China; University of Chinese Academy of Sciences, Beijing 100049, P.R. China

Huaijun Ma – State Key Laboratory of Catalysis, Dalian National Laboratory for Clean Energy, Dalian Institute of Chemical Physics, Chinese Academy of Sciences, Dalian 116023, P.R. China

Dongge Wang – State Key Laboratory of Catalysis, Dalian National Laboratory for Clean Energy, Dalian Institute of Chemical Physics, Chinese Academy of Sciences, Dalian 116023, P.R. China

Lin Wang – State Key Laboratory of Catalysis, Dalian National Laboratory for Clean Energy, Dalian Institute of Chemical Physics, Chinese Academy of Sciences, Dalian 116023, P.R. China

Yiwen Yang – State Key Laboratory of Catalysis, Dalian National Laboratory for Clean Energy, Dalian Institute of Chemical Physics, Chinese Academy of Sciences, Dalian 116023, P.R. China; orcid.org/0000-0002-4968-5448

Jianqiang Han – State Key Laboratory of Catalysis, Dalian National Laboratory for Clean Energy, Dalian Institute of Chemical Physics, Chinese Academy of Sciences, Dalian 116023, P.R. China

Wei Qu – State Key Laboratory of Catalysis, Dalian National Laboratory for Clean Energy, Dalian Institute of Chemical Physics, Chinese Academy of Sciences, Dalian 116023, P.R. China

Lin Yang – State Key Laboratory of Catalysis, Dalian National Laboratory for Clean Energy, Dalian Institute of Chemical Physics, Chinese Academy of Sciences, Dalian 116023, P.R. China; University of Chinese Academy of Sciences, Beijing 100049, P.R. China

Shuaiqi Wang – State Key Laboratory of Catalysis, Dalian National Laboratory for Clean Energy, Dalian Institute of Chemical Physics, Chinese Academy of Sciences, Dalian 116023, P.R. China; University of Chinese Academy of Sciences, Beijing 100049, P.R. China

Complete contact information is available at:

<https://pubs.acs.org/10.1021/acsomega.3c01174>

Notes

The authors declare no competing financial interest.

■ ACKNOWLEDGMENTS

This work was funded by the National Natural Science Foundation of China (grant no. 22272168) and the Dalian Institute of Chemical Physics (grant no. DICP 1202235).

■ REFERENCES

- (1) Alimohammadi, S.; Zendehboudi, S.; James, L. A comprehensive review of asphaltene deposition in petroleum reservoirs: Theory, challenges, and tips. *Fuel* **2019**, *252*, 753–791.
- (2) Shi, Q.; Zhao, S.; Zhou, Y.; Gao, J.; Xu, C. Development of heavy oil upgrading technologies in China. *Rev. Chem. Eng.* **2020**, *36*, 1–19.
- (3) Liu, B.; Zhao, K.; Chai, Y.; Li, Y.; Liu, D.; Liu, Y.; Liu, C. Slurry phase hydrocracking of vacuum residue in the presence of presulfided oil-soluble MoS₂ catalyst. *Fuel* **2019**, *246*, 133–140.
- (4) Sahu, R.; Song, B. J.; Im, J. S.; Jeon, Y.-P.; Lee, C. W. A review of recent advances in catalytic hydrocracking of heavy residues. *J. Ind. Eng. Chem.* **2015**, *27*, 12–24.
- (5) Zhang, S.; Liu, D.; Deng, W.; Que, G. A Review of Slurry-Phase Hydrocracking Heavy Oil Technology. *Energy Fuels* **2007**, *21*, 3057–3062.
- (6) Daage, M.; Chianelli, R. R. Structure-Function Relations in Molybdenum Sulfide Catalysts - the Rim-Edge Model. *J. Catal.* **1994**, *149*, 414–427.
- (7) Xie, J.; Zhang, H.; Li, S.; Wang, R.; Sun, X.; Zhou, M.; Zhou, J.; Lou, X. W.; Xie, Y. Defect-rich MoS₂ ultrathin nanosheets with additional active edge sites for enhanced electrocatalytic hydrogen evolution. *Adv. Mater.* **2013**, *25*, 5807–5813.
- (8) Kim, S. H.; Kim, K. D.; Lee, Y. K. Effects of dispersed MoS₂ catalysts and reaction conditions on slurry phase hydrocracking of vacuum residue. *J. Catal.* **2017**, *347*, 127–137.
- (9) Tye, C. T.; Smith, K. J. Cold Lake bitumen upgrading using exfoliated MoS₂. *Catal. Lett.* **2004**, *95*, 203–209.
- (10) Zheng, A.; Wang, D.; Wang, L.; Han, J.; Ma, H.; Pan, Z.; Qu, W.; Wang, C.; Tian, Z. Highly Efficient MoS₂ Nanocatalysts for Slurry-Phase Hydrogenation of Unconventional Feedstocks into Fuels. *Energy Fuels* **2021**, *35*, 2590–2601.

- (11) Sun, G.; Liu, D.; Li, M.; Tao, S.; Guan, Z.; Chen, Y.; Liu, S.; Du, Q.; Guo, H.; Yuan, X.; et al. Atomic coordination structural dynamic evolution of single-atom Mo catalyst for promoting H₂ activation in slurry phase hydrocracking. *Sci. Bull.* **2023**, *68*, 503–515.
- (12) Mitchell, D. L.; Speight, J. G. The solubility of asphaltenes in hydrocarbon solvents. *Fuel* **1973**, *52*, 149–152.
- (13) Adams, J. J. Asphaltene Adsorption, a Literature Review. *Energy Fuels* **2014**, *28*, 2831–2856.
- (14) Chen, Z.; Zhang, L.; Zhao, S.; Shi, Q.; Xu, C. Molecular structure and association behavior of petroleum asphaltene. In *Structure and Modeling of Complex Petroleum Mixtures*; 2015; pp. 1–38.
- (15) Groenzin, H.; Mullins, O. C. Asphaltene Molecular Size and Structure. *J. Phys. Chem. A* **1999**, *103*, 11237–11245.
- (16) Li, M.; Ren, T.; Sun, Y.; Xiao, S.; Wang, Y.; Lu, M.; Zhang, S.; Du, K. New parameter derived from the Hansen solubility parameter used to evaluate the solubility of asphaltene in solvent. *ACS Omega* **2022**, *7*, 13801–13807.
- (17) Ancheyta, J. *Asphaltenes: chemical transformation during hydroprocessing of heavy oils*; CRC press, 2010, DOI: 10.1201/9781420066319
- (18) Chen, L.; Bertolini, A.; Dubost, F.; Achourov, V.; Betancourt, S.; Cañas, J. A.; Dumont, H.; Pomerantz, A. E.; Mullins, O. C. Yen–Mullins Model Applies to Oilfield Reservoirs. *Energy Fuels* **2020**, *34*, 14074–14093.
- (19) Dickie, J. P.; Yen, T. F. Macrostructures of the asphaltic fractions by various instrumental methods. *Anal. Chem.* **1967**, *39*, 1847–1852.
- (20) Mullins, O. C. The Modified Yen Model. *Energy Fuels* **2010**, *24*, 2179–2207.
- (21) Yen, T. F.; Erdman, J. G.; Pollack, S. S. Investigation of the Structure of Petroleum Asphaltenes by X-Ray Diffraction. *Anal. Chem.* **1961**, *33*, 1587–1594.
- (22) Artok, L.; Su, Y.; Hirose, Y.; Hosokawa, M.; Murata, S.; Nomura, M. Structure and Reactivity of Petroleum-Derived Asphaltene. *Energy Fuels* **1999**, *13*, 287–296.
- (23) Schuler, B.; Meyer, G.; Peña, D.; Mullins, O. C.; Gross, L. Unraveling the Molecular Structures of Asphaltenes by Atomic Force Microscopy. *J. Am. Chem. Soc.* **2015**, *137*, 9870–9876.
- (24) Smith, D. F.; Podgorski, D. C.; Rodgers, R. P.; Blakney, G. T.; Hendrickson, C. L. 21 Tesla FT-ICR Mass Spectrometer for Ultrahigh-Resolution Analysis of Complex Organic Mixtures. *Anal. Chem.* **2018**, *90*, 2041–2047.
- (25) Mullins, O. C.; Sabbah, H.; Eyssautier, J.; Pomerantz, A. E.; Barré, L.; Andrews, A. B.; Ruiz-Morales, Y.; Mostowfi, F.; McFarlane, R.; Goual, L.; et al. Advances in Asphaltene Science and the Yen–Mullins Model. *Energy Fuels* **2012**, *26*, 3986–4003.
- (26) Nguyen, M. T.; Nguyen, D. L. T.; Xia, C. L.; Nguyen, T. B.; Shokouhimehr, M.; Sana, S. S.; Grace, A. N.; Aghbashlo, M.; Tabatabaei, M.; Sonne, C.; Kim, S. Y.; Lam, S. S.; le, Q. V. Recent advances in asphaltene transformation in heavy oil hydroprocessing: Progress, challenges, and future perspectives. *Fuel Process. Technol.* **2021**, *213*, No. 106681.
- (27) Alvarez-Ramírez, F.; Ruiz-Morales, Y. Island versus Archipelago Architecture for Asphaltenes: Polycyclic Aromatic Hydrocarbon Dimer Theoretical Studies. *Energy Fuels* **2013**, *27*, 1791–1808.
- (28) Chacón-Patiño, M. L.; Rowland, S. M.; Rodgers, R. P. Advances in Asphaltene Petroleomics. Part 1: Asphaltenes Are Composed of Abundant Island and Archipelago Structural Motifs. *Energy Fuels* **2017**, *31*, 13509–13518.
- (29) Cheng, X.; Zha, Q.; Zhong, J.; Yang, X. Needle coke formation derived from co-carbonization of ethylene tar pitch and polystyrene. *Fuel* **2009**, *88*, 2188–2192.
- (30) Redelius, P.; Soenen, H. Relation between bitumen chemistry and performance. *Fuel* **2015**, *140*, 34–43.
- (31) Dickinson, E. M. Structural comparison of petroleum fractions using proton and ¹³C n.m.r. spectroscopy. *Fuel* **1980**, *59*, 290–294.
- (32) Dereppe, J. M.; Moreaux, C.; Castex, H. Analysis of Asphaltenes by Carbon and Proton Nuclear Magnetic-Resonance Spectroscopy. *Fuel* **1978**, *57*, 435–441.
- (33) Sun, Z. H.; Li, D.; Ma, H. X.; Tian, P. P.; Li, X. K.; Li, W. H.; Zhu, Y. H. Characterization of asphaltene isolated from low-temperature coal tar. *Fuel Process. Technol.* **2015**, *138*, 413–418.
- (34) Trejo, F.; Ancheyta, J.; Rana, M. S. Structural Characterization of Asphaltenes Obtained from Hydroprocessed Crude Oils by SEM and TEM. *Energy Fuels* **2009**, *23*, 429–439.
- (35) AlHumaidan, F. S.; Hauser, A.; Rana, M. S.; Lababidi, H. M. S.; Behbehani, M. Changes in asphaltene structure during thermal cracking of residual oils: XRD study. *Fuel* **2015**, *150*, 558–564.
- (36) Seshadri, K. S.; Young, D. C.; Cronauer, D. C. Characterization of coal liquids by ¹³C n.m.r. and FT-i.r. spectroscopy — fractions of oils of SRC-I and asphaltenes and preasphaltenes of SRC-I and SRC-II. *Fuel* **1985**, *64*, 22–28.
- (37) Christopher, J.; Sarpal, A. S.; Kapur, G. S.; Krishna, A.; Tyagi, B. R.; Jain, M. C.; Jain, S. K.; Bhatnagar, A. K. Chemical structure of bitumen-derived asphaltenes by nuclear magnetic resonance spectroscopy and X-ray diffractometry. *Fuel* **1996**, *75*, 999–1008.
- (38) Speight, J. G. *Heavy oil recovery and upgrading*; Gulf Professional Publishing, 2019, DOI: 10.1016/C2016-0-04682-X.
- (39) Du, H.; Liu, D.; Li, M.; Wu, P.; Yang, Y. Effects of the Temperature and Initial Hydrogen Pressure on the Isomerization Reaction in Heavy Oil Slurry-Phase Hydrocracking. *Energy Fuels* **2015**, *29*, 626–633.
- (40) Seki, H.; Kumata, F. Structural change of petroleum asphaltenes and resins by hydrodemetallization. *Energy Fuels* **2000**, *14*, 980–985.
- (41) Ancheyta, J.; Centeno, G.; Trejo, F.; Marroquín, G. Changes in Asphaltene Properties during Hydrotreating of Heavy Crudes. *Energy Fuels* **2003**, *17*, 1233–1238.